TRANSPORT AIRCRAFT AERODYNAMIC IMPROVEMENT BY NUMERICAL OPTIMIZATION*

D. Destarac and J. Reneaux
Office National d'Etudes et de Recherches Aérospatiales (ONERA)
92320 Châtillon France

*This work was supported by Aerospatiale (Aircraft Division) and by the STPA

Abstract

Various applications of numerical optimization to the aerodynamic improvement of transport aircraft are presented from airfoil to wing design and control of interference phenomena. The method associates the CONMIN constrained minimization code with 2D and 3D aerodynamic programs. In 2D, the case of two airfoil designs in the same operating conditions but with geometric constraints corresponding to two alternative wing structures illustrates the usefulness of numerical optimization when geometrical control is required. In 3D, possibilities of wing drag minimization are shown, drag being splitted into its basic components to ensure better reliability of the objective calculations and more control in the design procedure. Finally, an example is given of minimization of wing/power plant interference effects on a four-engined jet aircraft, a problem for which numerical optimization is a promising approach.

Introduction

Numerical optimization can be useful to the aerodynamicist at different stages of wing design. In the first place, it can be applied to the design of the basic airfoil for the outer part of the wing where the flow is expected to be quasi-2D. One usually tries to minimize drag for a given lift value, or drag-to-lift ratio, while respecting geometric constraints (for structural reasons mainly) and possibly also aerodynamic constraints. When the basic airfoil has been defined, numerical optimization may be used to determine the twist distribution giving minimum drag, and also to control 3D phenomena which are unavoidable on a wing operating in transonic conditions ; such phenomena are liable to deteriorate the intrinsic qualities of the airfoil. Finally, if the wing is subject to interference from other components such as the engines, unfavourable interference effects can be minimized by numerical optimization. The purpose of this paper is to give examples of these various applications.

A unique constrainted minimization code can be used for the different applications considered, but the aerodynamic code obviously depends on the application. In all cases it ought to be fast and yet able to compute objective and constraint functions without numerical noise so as to avoid misleading gradient calculations. For an airfoil, such requirements can be met by 2D viscous-inviscid coupling methods using fine grids. For a wing they imply using coarse meshes and, in the example presented in this paper, an inviscid flow method. Accurate estimation of the aerodynamic coefficients is thus made more difficult, especially where drag is concerned. For a multicomponent configuration, drag cannot reasonably enter into the definition of the objective or constraint functions, and it is necessary to resort to simplified procedures such as the one presented in this paper.

Numerical optimization method

The principles of the method

An aerodynamic numerical optimization method consists of the association of three elements : a constrained minimization code, a direct aerodynamic code and a shape modification technique.

The designer must express the design aim and requirements in the form of numerical functions. The constrained minimization code will be used to minimize one of these functions (the objective) while the others (the constraints) will be kept below given values. Constraints are natural expressions of design requirements, either aerodynamic or geometrical, and the objective is usually closely related to the overall aerodynamic efficiency.

The designer must also define basic shape modifications which efficiently affect the objective and constraint functions. If $(Mod_i)_{i=1,n}$ represent the basic shape modifications, the designed shape DS_h is derived from the initial shape IS_h as :

$$DS_h = IS_h + \sum_{i=1}^{n} X_i \, Mod_i$$ where $(X_i)_{i=1,n}$ are the design variables. The basic modifications define the space in which the solution will be sought, and must be carefully chosen. Pleonastic shape functions will needlessly increase the cost of the optimization, whereas too few functions will lead to mediocre results.

The task of the minimization code is to calculate the design variables which minimize the objective function while respecting the given constraints..

The objective and constraint functions of an aerodynamic nature are calculated by a direct analysis code. This code must have three qualities :

- it must give theoretically sound estimations of the objective and constraint functions ;
- it must not introduce numerical noise into the calculation of the gradients of these functions which would be dangerously misleading to the minimization code ;
- it must be fast since an optimization process may require many direct aerodynamic calculations.

The elements of the method

The method used in the applications presented in this paper associates one constrained minimization code with two aerodynamic codes (one for 2D cases, the other for 3D) and several shape modification techniques depending on the problem being solved.

The minimization code is the well-known CONMIN program of Vanderplaats[1]. In the process of minimizing the objective OBJ $(\overline{X})$ while respecting constraints $G_j(\overline{X}) \leq 0, j = 1,..., m$, the design variable vector $\overline{X}$ is iteratively calculated via the formula : $\overline{X}_q = \overline{X}_{q-1} + \alpha^* \overline{S}_q$. $\overline{S}_q$, the search direction, is determined in the first stage of the iteration. In the second stage, the modulus α^* of the displacement in the search direction is calculated. How the search direction is determined depends on the state of the constraints. The constraint $G_j(\overline{X}) < 0$ is said to be active if $-\varepsilon \leq G_j(\overline{X}) \leq \varepsilon$, $\varepsilon > 0$, violated it $\varepsilon < G_j(\overline{X})$ and non-active if $G_j(\overline{X}) < -\varepsilon$. When all constraints are non-active, $\overline{S}_q$ is calculated by the steepest descent method in the first iteration. In the following iterations, CONMIN uses the Fletcher-Reeves conjugate gradient method, but the possibility of using a quasi-Newton method has been introduced. Otherwise, i.e. if any constraint must be considered, the method of feasible directions is used. The optimum displacement modulus α^* is determined using a polynomial approximation which in most cases demands three successive calculations. Since the determination of $\overline{S}_q$, regardless of the method used, requires knowledge of the gradients of the objective and constraint functions, which are calculated by finite differences, one iteration generally requires about n + 3 direct calculations, n being the number of design variables.

The optimization method presented in this paper calls for either an airfoil or a wing aerodynamic analysis code.

The 2D code models viscous transonic flow around airfoils. It was developed by J. Bousquet[2] at Aerospatiale by coupling a Garabedian and Korn non-conservative full potential equation solver and a Michel integral laminar / turbulent boundary layer method. Viscous interaction is weak and does not allow accurate calculation of separated flow configurations, but in practice constraints can make use of the method capability for predicting separation. "O" type meshes of 160 × 30 points are used. Drag is determined as the sum of the skin friction, viscous pressure and wave drag components.

When optimizing wings, Bredif's convervative full potential equation solver is used[3]. The discretisation is finite element and the algorithm, a fast preconditioned conjugate gradient method. Viscous effects are not modelled. Pressure drag is calculated by surface integration, and wave drag and lift-induced drag by "far field" momentum integrations. Whereas in 2D it is possible to get well converged solutions on fine meshes in little time, this is impossible in 3D. To keep the computation time within a reasonable limit (around 1' CPU per direct calculation on CRAY-XMP) one must give up either full convergence or mesh refinement. There is no doubt that full convergence is essential for avoiding numerical noise in the estimation of the objective and constraint gradients[4] : coarse grids must therefore be used (about 13000 points in the present case). Absolute values of the objective and constraint functions are necessarily inaccurate on such grids, but if the gradients are accurate enough this does not preclude correct optimization[5].

To modify airfoils, three classes of shape functions may be distinguished by their degree of aerodynamic meaning :

a) analytical functions have no aerodynamic meaning but they have the advantage of generality ;
b) some aerodynamic meaning can be obtained by using airfoil libraries ;
c) however, the most effective aerodynamic control is provided by aerofunctions, i.e. functions of pure aerodynamic origin[6].

Theoretically the three classes may be used in 3D as well although in practice the fact that fewer design variables are necessary with aerofunctions makes these the most suitable for expensive 3D optimizations. Wing optimizations presented in this paper use aerofunctions to modify wing sections and also modifications of the twist distribution, but not of the the planform.

Supercritical airfoil design by numerical optimization

Aerodynamic studies on basic airfoils for transport aircraft wing design seek a good compromise between aerodynamic efficiency (lift-to-drag ratio, drag-rise limits, etc.) and structural constraints (thickness-to-chord ratio, thickness at spar locations, etc.).

For supercritical airfoils, the main features to be optimized in cruise conditions are the following :

- extent of the supersonic area, and Mach number upstream of the shock which control wave-drag at cruise and drag-rise limits ;
- upper surface pressure recovery in order to avoid boundary-layer separation close to the trailing-edge ;
- intensity of rear-loading in order to adapt the airfoil to high lift coefficients while controlling pitching moment.

Among existing methods, numerical optimization seems well suited to these types of design problems. It makes it possible to simultaneously control global coefficients (C_L, C_D, C_m), pressure distributions, boundary-layer characteristics, and airfoil geometry[7].

As an example, the design of two supercritical airfoils for a transport aircraft wing by numerical optimization is presented. Design conditions are $M = 0.73$, $C_L \sim 0.7$ and $Re = 6.10^6$, transition being enforced at 7 % of the chord. The two airfoils were designed with different wing technology options in view. Airfoil A had to respect three geometrical constraints : maximum relative thickness $e/c \geq 12.3$ % and thickness at the locations of spars e/c (20 %) ≥ 11.3 %, e/c (65 %) ≥ 7.7 %. In the case of airfoil B, these constraints were changed : thickness at 20 % of the chord was not controlled while a more severe constraint was enforced at 65 % : x/c (65 %) ≥ 8.9 %.

In both cases, the optimization made use of airfoil libraries. The coordinates of the current airfoil are defined as :

$$\overline{Y} = \overline{Y}_0 + X_1 (\overline{Y}_1 - \overline{Y}_0) + .,. + X_n (\overline{Y}_n - \overline{Y}_0)$$

$\overline{Y}_0$ being the initial airfoil and $(X_1,..., X_n)$ the design variables. Each airfoil of the library thus belongs to the solution search space.

The elements of the libraries used for these optimizations were existing supercritical airfoils with modified thickness distributions so as to respect the geometrical constraints although the upper surfaces were unchanged to preserve the supercritical quality. This allows automatic respect of geometrical constraints and the optimization problem may be simply formulated as :

objective : • $C_D (M_0)$
constraints : • $C_L \geq C_{L_0}$
• $|C_m| \leq C_{m_0}$
• no separation

For each airfoil, several optimization calculations were performed using different shape libraries and moving the design conditions around the specified point M_0, C_{L_0} ($0.73 \leq M_0 \leq 0.75$, $0.60 \leq C_{L_0} \leq 0.80$). The final choice between the results of these calculations was made taking into account the efficiency in cruise conditions and off-design behaviour : drag-rise and buffeting limits. Drag rise was determined by the rule $\partial C_D/\partial M = 0.10$ and buffeting onset by the criterion of Mach number upstream of the shock equal to 1.3.

Pressure distributions calculated by the aerodynamic code used for the optimization are presented in Figure 1 for both optimized airfoils ; they differ mainly on the lower surface. Upper surface pressure distributions are close, airfoil B having a slightly weaker shock. Also in Figure 1, C_L versus C_D curves calculated by the same code show that for both airfoils C_L/C_D is maximum around $C_L = 0.7$.

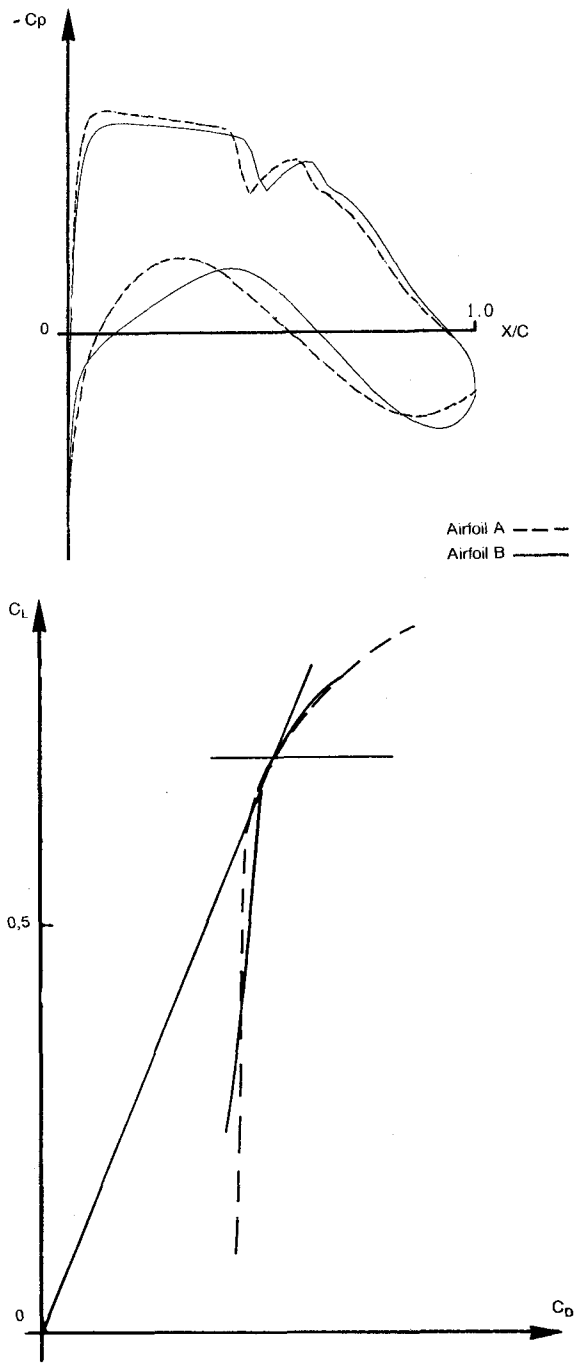

Fig. 1 - Supercritical airfoil design. Computed aerodynamic characteristics. $M = 0.73, C_L = 0.70, Re = 6.10^6$.

Aerodynamic characteristics were experimentally checked in ONERA's S3MA wind-tunnel. The results are shown in Figure 2. As predicted by the calculations, maximum lift-to-drag ratio is obtained at $C_L = 0.7$ for both airfoils ; with regard to drag rise, airfoil B is slightly better. The separation limit was determined by examining trailing-edge pressure and did not show any significant difference between the two airfoils. Finally, Figure 3 compares measured pressure distributions for the two airfoils at the design point. Globally-speaking, it reflects the computational predictions, although not exactly as concerns the shock locations.

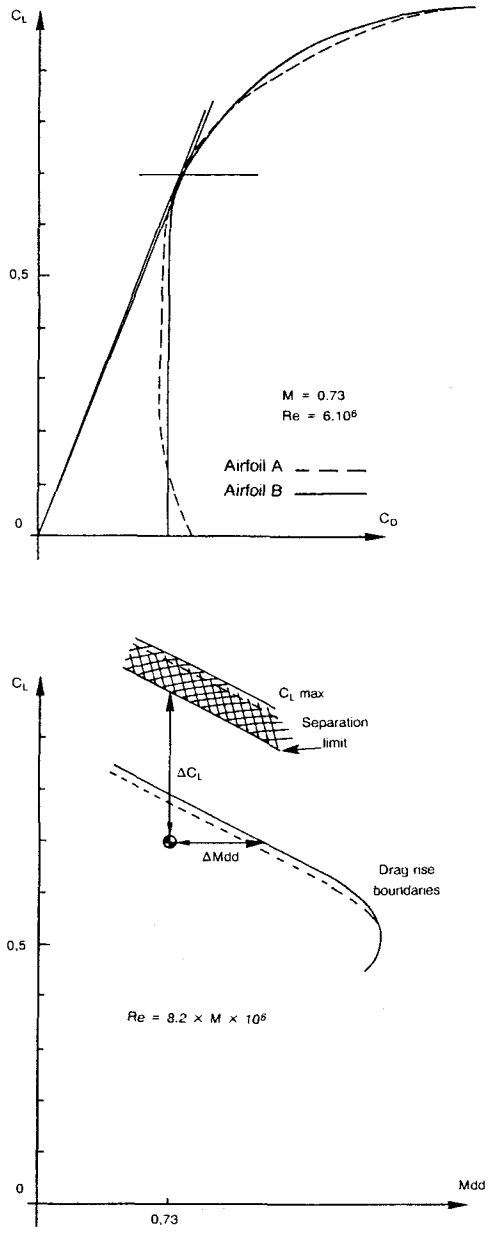

Fig. 2 - Supercritical airfoil design. Aerodynamic characteristics measured in S3MA.

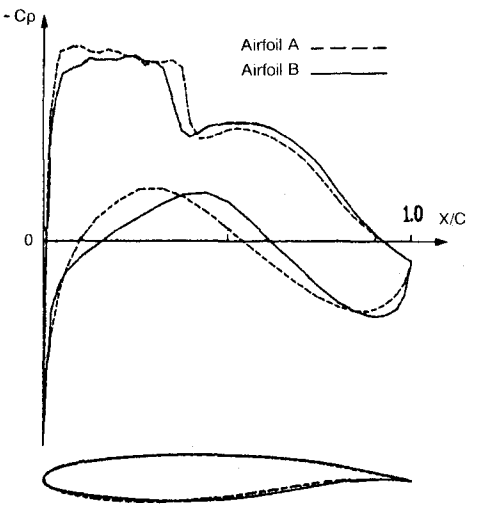

Fig. 3 - Supercritical airfoil design. Pressure distributions measured in S3MA at $M = 0.73, C_L = 0.70, Re = 6.10^6$.

Both airfoils fulfilled the prescribed aerodynamic requirements. Airfoil B was preferred to airfoil A to generate a supercritical wing operating at M = 0.82, $C_L = 0.47$. Apart from a slight aerodynamic advantage in drag-rise limit, its geometrical characteristics allow more gain in weight and more space for the outer wing jacks.

In this example, numerical optimization allowed fast airfoil design taking into account both aerodynamic and geometrical requirements. Experimental checking was satisfactory.

Wing drag reduction by numerical optimization

Drag minimization is all the more difficult since drag prediction itself is no easy matter[8, 9]. It is indeed impossible to compute drag with accuracy on coarse grids. Although refined meshes are acceptable in 2D optimization, computation time forbids their use in 3D problems since one optimization requires seldom less than 50 direct calculations in realistic cases. In spite of this dilemma, the optimization technique has been successfully applied to wing drag minimization by several authors [4, 5]. In fact, one of these authors showed that successful optimization requires only accuracy of drag increments, and not necessarily absolute drag accuracy[11].

Estimating drag by "far-field" techniques is generally acknowledged to be more accurate than "near-field" integrations[9, 10]. It is also more useful because it distinguishes between the different physical sources of drag, thus giving more information to the aerodynamicist and more control to the designer.

The purpose of the following calculations is to show some of the possibilities of this technique in optimization. The aerodynamic code solving the full potential equation, only inviscid drag components will be considered (lift-induced and wave drag).

The two optimization cases presented here make use of the DLR-F4 research wing. An account of this wing's design may be found in reference[12]. This typical subsonic transport aircraft wing is sketched in Figure 4. It is defined by only four spanwise sections, the same supercritical airfoil being used in the outer three sections with different twist values. The twist distribution is linear between the definition sections.

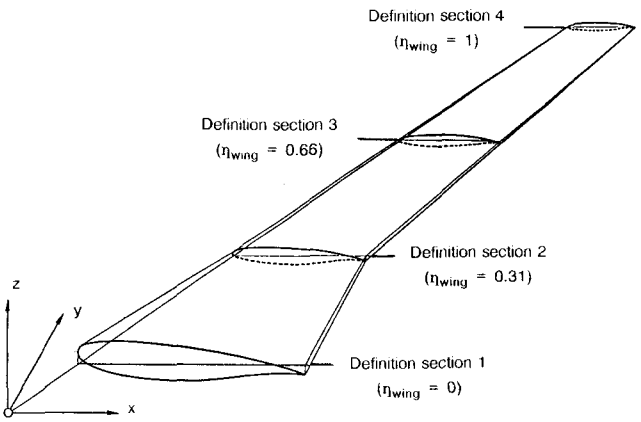

Fig. 4 - DLR - F4 wing.

In the first case we first untwisted the wing and then tried to optimize the twist distribution. There are four design variables : the twist angles in the four sections. The reference flow conditions considered are M = 0.75, C_L = 0.67. Optimization calculations were performed with different objective functions and the constraint $C_L \geq 0.67$. They are summed up in Table 1. The objective functions chosen were : 1) lift-induced drag, 2) wave drag, 3) lift-induced + wave drag, 4) pressure drag, and 5) an additional unconstrained calculation was done aiming at an elliptical load distribution.

		C_{D_i} ($\times 10^4$)	C_{D_w} ($\times 10^4$)	$C_{D_i} + C_{D_w}$ ($\times 10^4$)	C_{D_p} ($\times 10^4$)
F4 wing		199.1	21.3	220.4	255.2
Initial untwisted wing		203.9	33.3	237.2	267.3
Calculation	Objective	C_{D_i} ($\times 10^4$)	C_{D_w} ($\times 10^4$)	$C_{D_i} + C_{D_w}$ ($\times 10^4$)	C_{D_p} ($\times 10^4$)
1	C_{D_i}	197.6	24.1	221.7	256.3
2	C_{D_w}	204.5	21.1	225.6	258.7
3	$C_{D_i} + C_{D_w}$	197.9	22.7	220.6	255.0
4	C_{D_p}	198.4	22.4	220.8	254.9
5	Elliptical load	197.5	23.8	221.3	255.8

Table I - Drag minimization by wing-twist optimization.

Results will first be discussed in terms of load distributions. Figure 5 shows that minimizing lift-induced drag (calculation 1), starting from the untwisted wing heavily loaded in the outer part, brings the load distribution close to being elliptical as should be expected. And yet the ellipse is imperfectly obtained. An exact elliptical distribution was procured in calculation 5 by minimizing the difference between the load distribution and an ellipse. Table 1 shows that the lift-induced drag thus obtained is C_{D_i} = 197.5.10^{-4} to be compared to C_{D_i} = 197.6.10^{-4} by minimizing this coefficient. The conclusion is that calculation 1 stops in a relative minimum probably very close to the absolute.

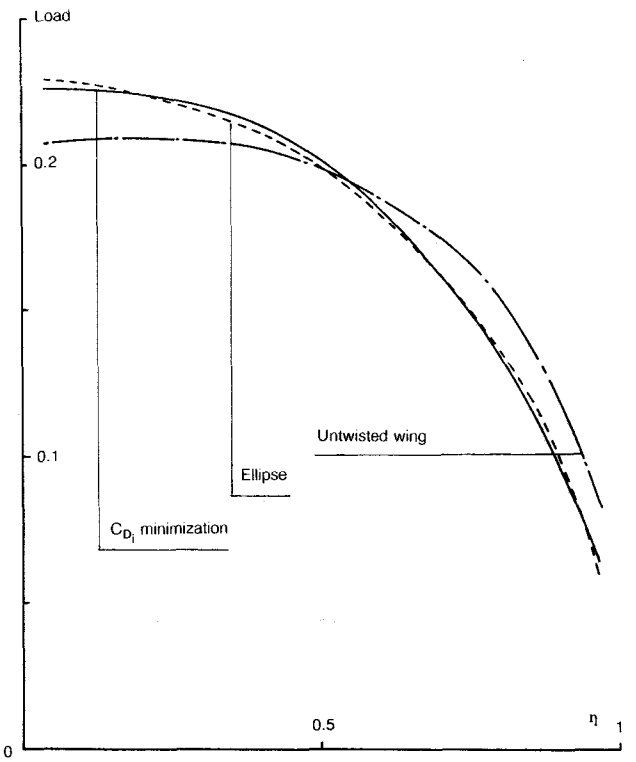

Fig. 5 - Wing twist optimization for lift-induced drag minimization (M = 0.75, C_L = 0.67). Spanwise load distributions.

In calculation 2, wave drag is minimized regardless of lift-induced drag. Figure 6 shows that the wing with minimum wave drag is heavily loaded in the inner part. A very unelliptical load distribution is obtained, creating muchlift-induced drag as indicated in Table 1.

Calculation 3 is the minimization of the sum of lift-induced drag and wave drag. It consistently leads to a load distribution lying between the two previous ones (Figure 6). Compared to the real F4 wing, this wing has less lift-induced drag and more wave drag. The sum of the two is slightly smaller in the case of F4 (220.4.10^{-4} versus 220.6.10^{-4}) : the solution obtained is not strictly an optimum.

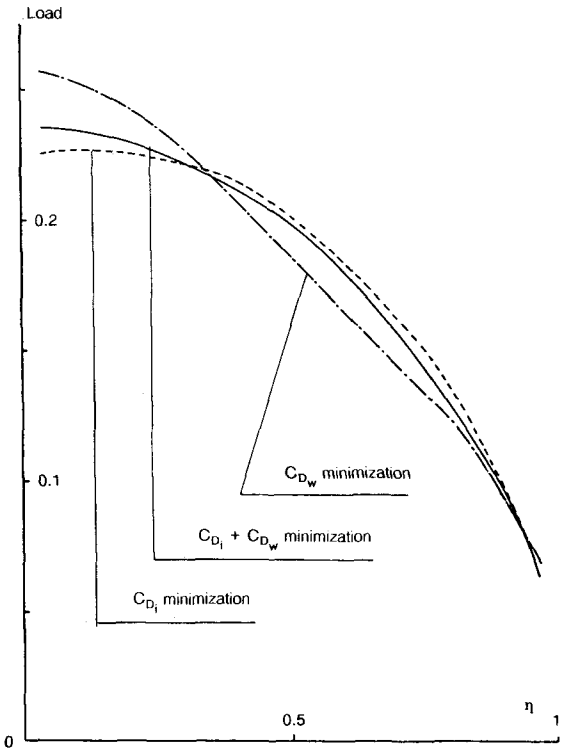

Fig. 6 - Wing twist optimization for drag minimization ($M = 0.75, C_L = 0.67$). Spanwise load distributions.

In inviscid flow pressure drag is theoretically equal to the sum of lift-induced drag and wave drag. Yet the fact that we do find almost identical solutions by minimizing these two quantities, as shown in Figure 7, does not go without saying, owing to the notion that "near-field" integration is less accurate than "far-field" techniques. Indeed, in all the cases presented in Table 1, C_{D_p} values are much higher than $C_{D_i} + C_{D_w}$. But the increments are more or less in agreement. No evidence of a relative minimum is perceptible in this case, whether we compare to the F4 or to calculation 3.

By minimizing total inviscid drag (calculations 3 and 4), we do not find the twist distribution of the real F4 wing. But one must realize that the result greatly depends on the operating point chosen for the optimization. Figure 8 shows that by minimizing $C_{D_i} + C_{D_w}$ at M = 0.785 instead of M = 0.75, for the same load coefficient C_L =0.67, one obtains a twist distribution closer to the F4 (which in fact was designed for M = 0.78512). When the Mach number is increased, the balance of wave and lift-induced drag is altered, the wave component acquiring more weight in the total which changes the optimal twist distribution.

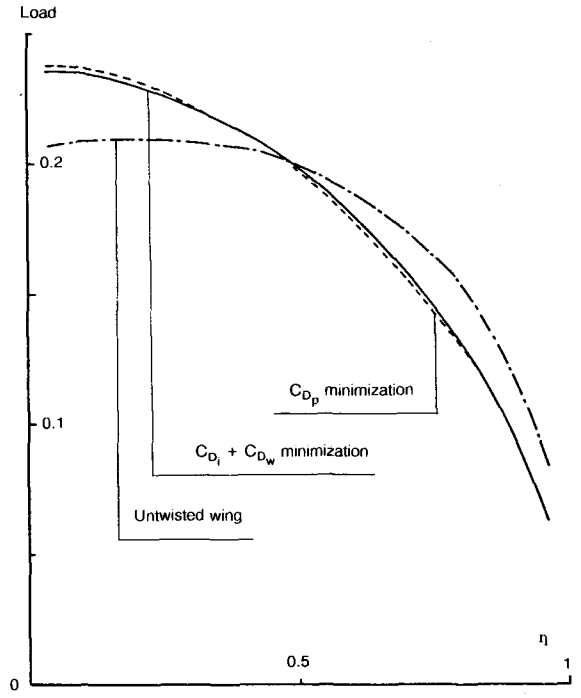

Fig. 7 - Wing twist optimization for total inviscid drag minimization ($M = 0.75, C_L = 0.67$). Spanwise load distributions.

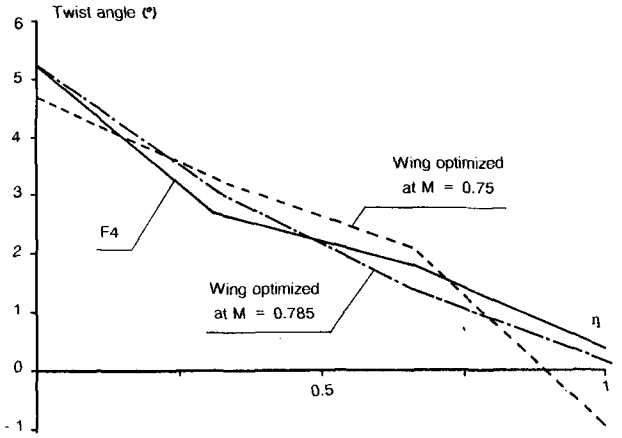

Fig. 8 - Wave + induced drag minimization at two operating points. Optimized twist distributions.

The second example shows how 3D numerical optimization may be used to solve a typical problem arising in transport aircraft wing design. A basic airfoil designed by 2D or quasi-2D methods is generally used in the outer part of the wing where (except close to the tip) the flow behaviour is quasi-2D. But in the inner part of the wing, owing to aerodynamic reasons (especially in transonic conditions) and aircraft design considerations (space for undercarriage, structural constraints, etc.), the flow is essentially 3D and the problem cannot be handled by 2D methods.

The wing to be optimized was derived from the F4 wing via the following procedure :

a) The three outer defining sections of the F4 wing were preserved, including their twist angles.

b) The root section was replaced by the basic airfoil.

c) The lower surface of this new root section was modified so that the thickness at 20 % and 65 % of the chord (typical spar locations) be that of the real F4 wing.

d) The root section twist angle was determined so as to give the same lift coefficient at the same angle of attack.

So this wing is basically defined by a unique airfoil with only a rough modification at the root to provide as much space there as in the case of the F4. Figure 9 shows that, at M = 0.785, C_L = 0.55, root section adaptation is badly needed. This adaptation was performed by numerical optimization.

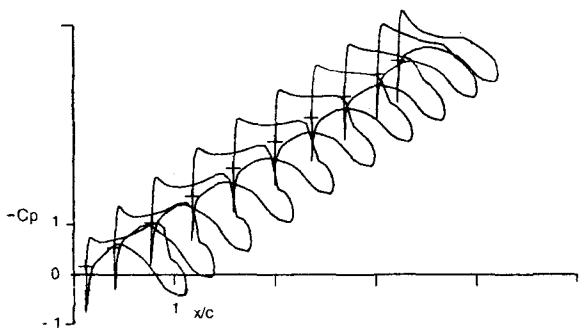

Fig. 9 - Initial wing for root section optimization ($M = 0.785, C_L = 0.55$).

The flow on the initial wing shows an unacceptable rear shock near the root. Three very simple basic shape functions were used for the optimization : 1) a modification of the camber line from 50 % to 100 % of the chord to control the rear shock ; 2) a modification of the camber line from 0 % to 50 % of the chord to likewise control a possible supersonic shock ; 3) the root section twist angle. These modifications do not allow to modify the chordwise thickness distribution. A constraint was enforced upon the lift coefficient : $C_L \geq 0.55$.

Two optimization calculations were carried out, calculation A with $C_{D_i} + C_{D_w}$ as the objective function, and calculation B with C_{D_p}. Table II shows that calculation A consistently leads to a wing with lower $C_{D_i} + C_{D_w}$ and higher C_{D_p} than calculation B.

Table II - Drag minimization by root-section optimization.

		C_{D_i} (× 10⁴)	C_{D_w} (× 10⁴)	$C_{D_i} + C_{D_w}$ (× 10⁴)	C_{D_p} (× 10⁴)
F4 wing		133.9	12.4	146.3	174.1
Initial wing		134.0	17.2	151.2	178.2
Calculation	Objective	C_{D_i} (× 10⁴)	C_{D_w} (× 10⁴)	$C_{D_i} + C_{D_w}$ (× 10⁴)	C_{D_p} (× 10⁴)
A	$C_{D_i} + C_{D_w}$	133.6	13.0	146.6	174.7
B	C_{D_p}	133.8	13.4	147.2	174.5

The problem is posed in such a way that C_{D_i} is not allowed to change much since there is a constraint upon C_L and the twist distribution from section 2 to the tip is not modified. So C_{D_w} obviously is the drag component that should be the most reduced by the optimization.

Such is the case in calculation A : wave drag reduction is dominant. The effect of the optimization on pressure distributions is shown in Figures 10 and 11. Rear shock strength has been greatly reduced in the root section and the favourable effect extends up to 60 % of the span although the wing was not modified past η = 0.31. All drag component levels are close to those of the real F4 wing (Table II) as is the shock strength, as shown in Figure 12. It must be noted that, contrary to the previous example, the real root section of the F4 wing was not in the solution search space and it is not surprising that a better wing than the F4 is not obtained considering the very simple basic shape modifications used.

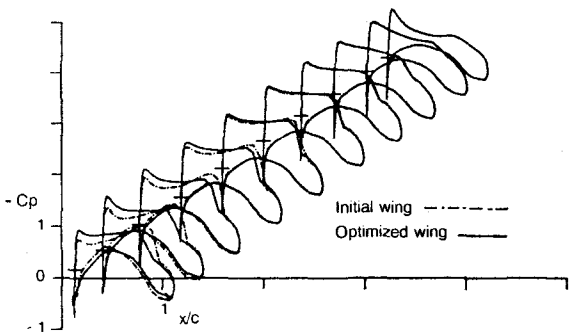

Fig. 10 - Root section optimization. $C_{D_i} + C_{D_w}$ minimization ($M = 0.785, C_L = 0.55$).

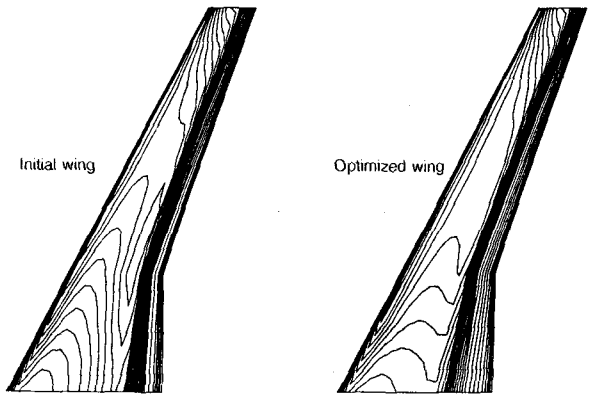

Fig. 11 - Root section optimization. $C_{D_i} + C_{D_w}$ minimization ($M = 0.785, C_L = 0.55$). Upper surface isobar lines ($\Delta Cp = 0.05$).

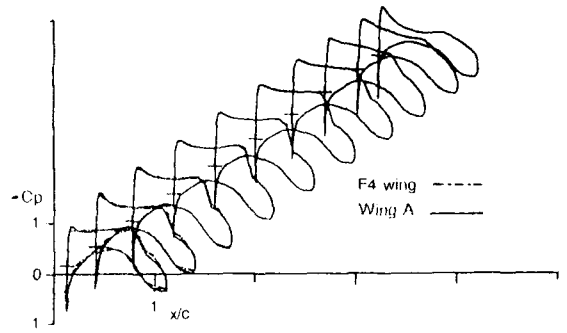

Fig. 12 - Root section optimization checking. $C_{D_i} + C_{D_w}$ minimization ($M = 0.785, C_L = 0.55$).

Wing B, obtained by minimizing C_{D_p}, is not as satisfactory. The comparison with wing A in Figure 13 shows that the shock strength has been insufficiently reduced. Since there is no evidence in Table II of a relative minimum having been reached, it must be concluded that, in this case, pressure drag is not estimated accurately enough to be used as an objective function. A similar result in another case in which wave drag was the key to successful optimization is presented in reference[13].

It should be noticed in Table II that drag increments between the different wings are underestimated, which does not help the minimization. When calculated on fine meshes they are about four times higher.

Drag estimated by "far-field" application of the momentum theorem appears to be a more reliable objective function in wing optimization than drag computed from the "near-field". The question of "how reliable ?" cannot be fully answered by simple examples such as those presented here. In particular, it may be questioned whether numerical optimization using coarse grids would be efficient or even correct when applied to a nearly optimal wing in order to find the real optimum, a case in which drag increments would be very small[14]. Moreover, the difficulty in distinguishing between a relative and an absolute minimum would be aggravated in such a problem.

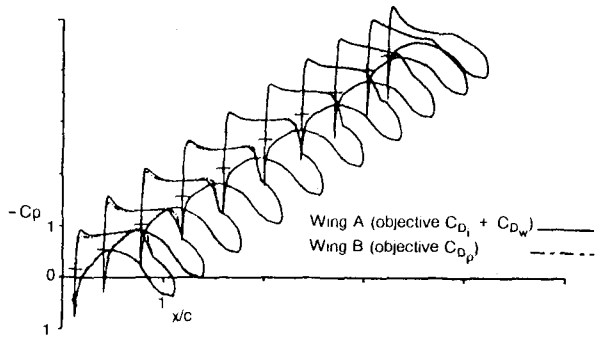

Fig. 13 - Root section optimization. $C_{D_i} + C_{D_w}$ vs C_{D_p} minimization ($M = 0.785, C_L = 0.55$).

Wing/engine interference reduction by numerical optimization

On most modern transport jets, the engines are mounted under the wing. The aerodynamic interference between these two components of the aircraft has unfavourable effects on its performance : at a given operating point (M, C_L), the wing/engine drag is greater than the sum of the wing drag and the engine drag. Optimization of a wing/engine configuration should aim at reducing the drag increment created by the interference. However, reliable estimation of this drag increment is still beyond the scope of analysis methods, let alone such inexpensive methods as might be incorporated into an optimization procedure.

The example presented here uses the following simplified methodology : one aims at averting the aerodynamic effect of the engine on the flow around the wing by modifying the wing shape in such a way that the flow on the motorized, optimized wing be as close as possible to the flow on the clean, original wing. This is illustrated by Figure 14 : the perturbation created by the engine is balanced by an opposed perturbation obtained through wing shape modifications. The perturbation of the pressure field on the wing to be balanced is determined "a priori", from experimental results and direct calculations of the original wing with and without engines (Figs. 14, a and b) by an analysis code capable of handling complex configurations. From there, a target pressure distribution on the wing alone is defined (Fig. 14, c) and the 3D optimization method can be used although it is restricted to wing alone optimization. The effect of the engine is not accounted for in the calculation of the objective function, but rather in the definition of this function. Finally the optimization result is checked

through direct calculation of the modified motorized wing using the previously mentioned analysis code (Fig. 14 d).

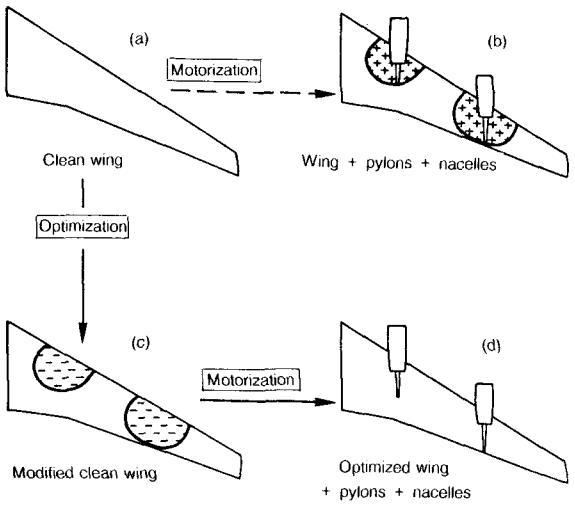

Fig. 14 - Optimization of a four-engined transport aircraft wing taking into account the effects of the propulsive system.

The wing adaptation presented here was carried out for a four-engined aircraft. The effects of the power plant (pylons + through-flow nacelles) on the wing were determined in a wind tunnel. Figure 15 shows measured pressure perturbations on the wing on both sides of each pylon. The outstanding phenomenon is a severe flow acceleration on the wing lower surface, on the inner side of each pylon. This brings about two drawbacks : the accelerated flow area ends with a shock wave, thus increasing wave drag, and it causes a lift deficit which must be made up for by a higher angle of attack, thus resulting in stronger shocks on the upper surface and again increased wave drag. The optimization must try to minimize this perturbation if not suppress it. On the outer sides of the pylons as well as on the upper surface, the perturbation is weaker and should be more easily removed by the optimization.

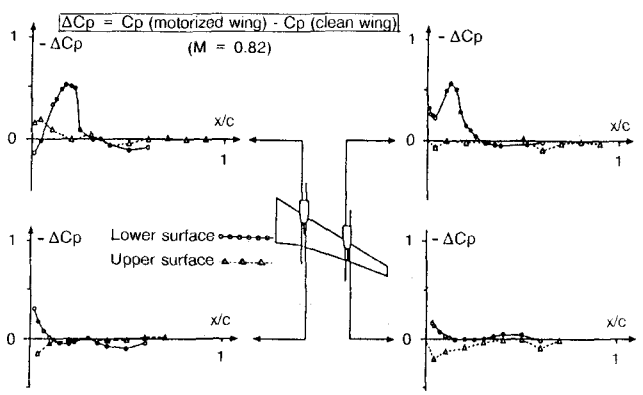

Fig. 15 - Aerodynamic effects of the propulsive system on the wing of a four-engined transport aircraft measured in wind tunnel.

The optimization is carried out in a manner which might be called "quasi-inverse" since the objective is to obtain a given pressure distribution, the objective function being a measure of the difference between the current pressure distribution and the target pressure distribution. Available wind tunnel results (Fig. 15) do not give any information about the spanwise extent of the perturbation. This has to be deduced from calculations of the wing with and without the power plant by means of a panel method. The calculated perturbation is shown in Figure 16. The objective functions are defined by target pressure distributions in the sections of the wing in which the perturbation is maximum, i.e., those in Figure 15. The spanwise extent of the phenomenon does not enter into the objective definition but into that of the shape functions : the wing shape is modified in the areas indicated in Figure 16, the shape alterations being maximum in the engine sections.

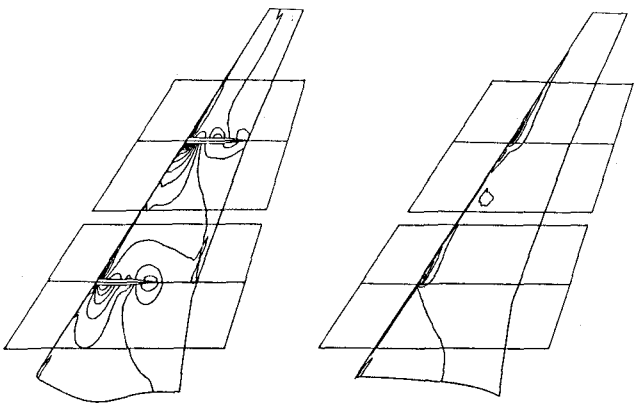

Fig. 16 - Four-engined transport aircraft wing optimization taking into account the effect of the propulsive system. Definition of the areas to be modified after panel calculations.

In so peculiar a problem it is necessary that the shape functions be defined bearing in mind the target of the optimization. For example, Figure 17 shows the shape functions chosen for the wing lower surface. Functions 1 to 7 are aerofunctions, defined by 2D inverse calculations so as to give extensive control over the whole lower surface with emphasis on the area where the perturbation is maximum (around 20 % of the chord). Function 8 is an homothetical form of the lower surface which allows control of the thickness. On the upper surface, only three shape functions were defined ; local twist was also used.

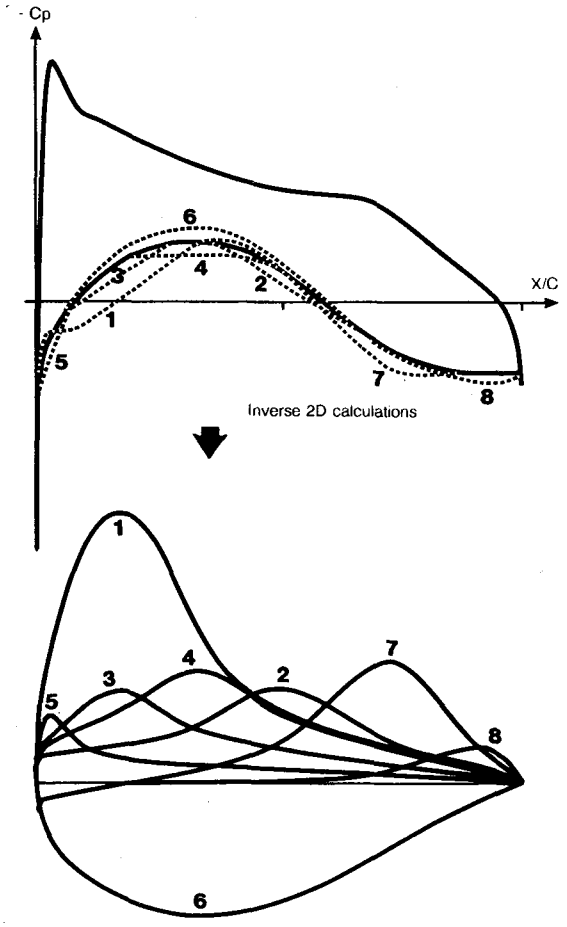

Fig. 17 - Examples of aerofunctions defined by 2D inverse calculations.

Figure 16 shows that the effect of the two engines does not overlap. The wing may thus be modified around each engine by separate optimization calculations. Moreover, the perturbation created by an engine is not symmetrical ; owing to the pylon, it is strongly discontinuous on the lower side of the wing as shown in Figures 15 and 16. The aerodynamic code used by the 3D optimization method is restricted to a wing alone and would thus smooth out the discontinuity. So the adaptation of the wing around each engine must be decomposed into two optimization calculations, one aiming at the target on the inner side, the other on the outer side. The two shape modifications are then fitted together inside the pylon thickness. The complete optimization thus requires four separate optimization calculations.

Let us consider the first and the fourth of these calculations. On the inner side of the inner engine, the prime objective of the adaptation must be to avoid a shock taking place at 20 % of the chord (Fig. 15) on the lower surface of the motorized wing. The chosen target pressure distribution is shown in Figure 18. It is defined on the lower surface of the wing only. The plateau around 20 % of the chord is not meant to be reached by the optimization, but to induce a trend in the right direction. Six shape functions were used on the lower surface, none on the upper surface nor the local twist. Optimization was carried out taking into account the wing thickness at the front spar location which is a simplified way of considering a structural constraint. The geometrical constraint is written so as to keep the thinning δ at 20 % of the chord within a prescribed limit. Several calculations were done with more or less severe constraints : $\delta \leq 0$ i.e., without allowing any thinning at the spar ; $\delta \leq 5$ % ; $\delta \leq 10$ % ; and lastly, a calculation without any geometrical constraint.

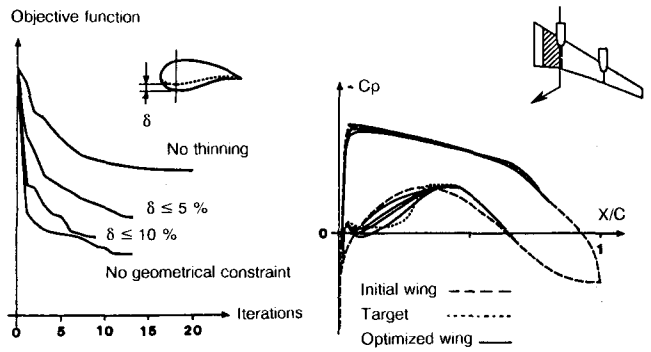

Fig. 18 - Optimization of a four-engined transport aircraft wing at M = 0.82 using 6 lower surface shape functions.

Figure 18 shows convergence and results of calculations with these various constraints. Some of the convergence graphs show steps : they appear when the target pressure distribution is reached on one part of the chord, then another, and so on. The optimized solution gets closer to the target when the constraint is loosened, because in this case the geometrical constraint directly hinders the aerodynamic effect sought through the objective definition. Only without constraint do we get a significant adaptation. Therefore the other three optimizations were made without geometrical constraints.

For example, the optimization on the outer side of the outer engine is presented in Figure 19. Here the target includes both upper and lower pressure distributions and 12 shape functions were used : 8 on the lower surface, 3 on the upper surface, and local twist. A satisfactory result is obtained in about 15 iterations. The peak on the convergence graph is due to manual modification of one of the design variables in order to get out of a relative minimum and accelerate final convergence. Such a procedure is sometimes used in practical optimization problems.

Strict checking of the optimization would require wind tunnel testing of the modified wing equipped with pylons and nacelles. The verification presented in Figure 20 is only approximate because it was made by computational means, whereas the objective of the optimization was defined using experimental data. The analysis method is the panel code previously employed

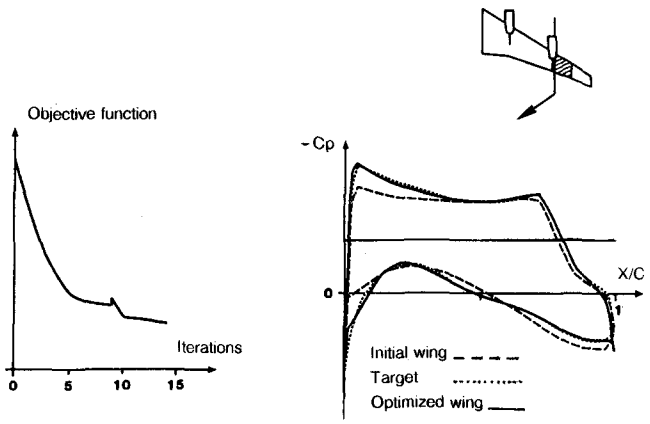

Fig. 19 - Optimization of a four-engined transport aircraft wing at M = 0.82 using 12 lower and upper surface shape functions.

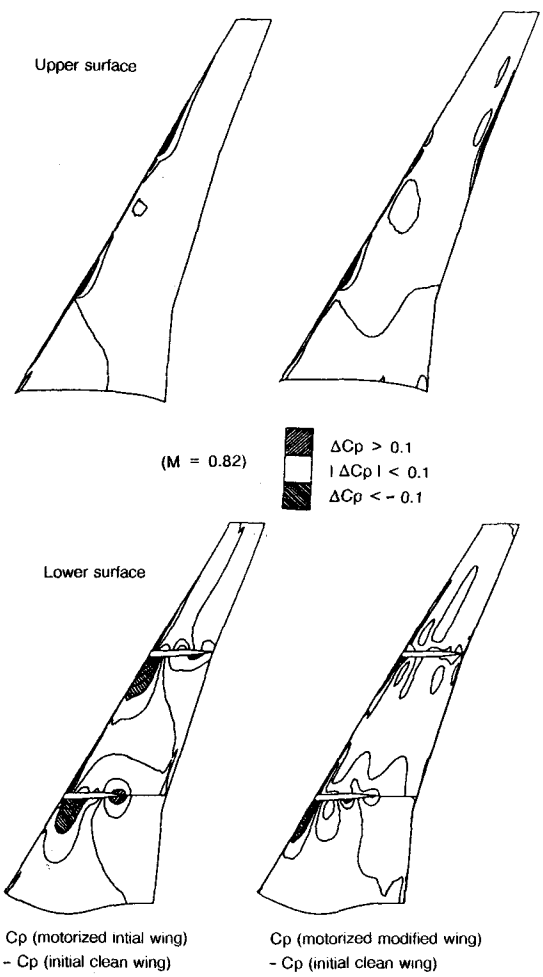

Fig. 20 - Four-engined transport aircraft wing optimization taking into account the aerodynamic perturbation by the propulsive system. Checking calculations (panel method).

to estimate the perturbation extent : neither shock waves nor viscous effects are taken into account. Figure 20 shows iso-ΔCp lines, ΔCp being the difference betweenCp on the motorized wing and Cp on the original clean wing. On the lower surface, the perturbation around the inner engine has been reduced ; in particular, there is no risk that a shock should arise at 20 % of the chord. Around the outer engine, the perturbation has been entirely suppressed. The upper surface was modified around the outer engine only. In a consistent manner, the outer perturbation has been suppressed.

Conclusion

In the application of numerical optimization to transport aircraft aerodynamic design, the state of the art at ONERA may be summed up as follows.

- For airfoil design, it has been widely and successfully used in concurrence with inverse methods.

- Acquiring the same reliability for wing design is still work in progress but should be achieved in not too remote a future.

- For multicomponent problems, simplified approaches are already possible ; these must be developed and completed inasmuch as interference phenomena are typical problems that should be handled by numerical optimization rather than other approaches.

As for the approach itself, notwithstanding its many successes, some inherent limitations and uncertainties should not be overlooked. Obtaining really optimal design through a numerical procedure instead of only improved design (or no improvement at all), requires three conditions :

- that the basic shape functions be general enough ;

- that the minimization code be able to find the absolute minimum in the space defined by the basic shape functions ;

- that the objective and constraint estimation be reliable.

The latter condition is the most stringent because the designer may enrich the shape function basis, or help the minimization by changing initial design variable values or perturbing them at some point of the calculation. But he can only trust the aerodynamic code. Therefore, progress in optimization greatly depends on progress in the ability to compute flows both accurately and economically.

Acknowledgements

The authors wish to thank Mr J.-J. Mirat and Mr D. Gisquet from Aerospatiale Aircraft Division for valuable help and stimulating discussions.

References

[1] G.N. Vanderplaats :
CONMIN, a FORTRAN Program for Constrained Function Minimization.
NASA TM X-62, 282-1973.

[2] J. Bousquet :
Calculs Bidimensionnels Transsoniques avec Couche Limite.
AAAF, 11ème Congrès d'Aérodynamique Appliquée, 1977.

[3] M. Brédif :
Finite Element Calculation of Potential FLow around Wings.
9ème Congrès International sur les Méthodes Numériques en Mécanique des Fluides, Saclay, juin 1983. Lecture Notes in Physics, Vol. 218, Springer Verlag 1985.

[4] R. Hicks, P.A. Henne :
Wing Design by Numerical Optimization
AIAA Paper 77-1247, Seattle, 1977.

[5] G.B. Cosentino, T.L. Holst :
Numerical Optimization Design of Advanced Transonic Wing Configurations.
Journal of Aircraft, Vol. 23, n° 3, March 1986, pp. 192-199.

[6] P.V. Aidala, W.H. Davis Jr., W.H. Mason :
Smart Aerodynamic Optimization.
AIAA Paper 83-1863, 1983.

[7] J. Reneaux, J.-J. Thibert :
The Use of Numerical Optimization for Airfoil Design.
AIAA Paper 85-5026, Colorado Springs, 1985.

[8] J.W. Slooff :
Computational Drag Analysis and Minimization, Mission Impossible ?
NLR MP 85080 U, 1985.

[9] J.W. Slooff :
Technical Status Review on Drag Prediction and Analysis from Computational Fluid Dynamics : State of the Art. Foreword and Conclusions.
AGARD Advisory Report No. 256, Lisbon, 1988.

[10] R.C. Lock :
Comment on "Numerical Optimization Design of Advanced Transonic Wing Configurations".
Journal of Aircraft, Vol. 24 n° 8, August 1987, p. 575.

[11] G.B. Cosentino, T.L. Holst :
Reply by Authors to R.C. Lock.
Journal of Aircraft, Vol. 24 n° 8, August 1987, pp. 575-576.

[12] G. Redeker, N. Schmidt, R. Müller :
Design and Experimental Verification of a Transonic Wing for a Transport Aircraft.
AGARD-CP-285, Paper n° 13, 1980.

[13] D. Destarac, J. Reneaux, D. Gisquet :
Optimisation Numérique de Voilures en Régime Transsonique.
AGARD-CP N° 463, Loen, Norway, 1989.

[14] Technical Evaluator's Remarks and Round Table Discussion on Computational Methods for Aerodynamic Design (Inverse) and Optimization.
AGARD-CP N° 463, Loen, Norway, 1989.